

High-pressure study of topological semimetals □Cd2Sb2 (□ = Eu and Yb)

Chuchu Zhu(朱楚楚)1, Hao Su(苏豪)2, Erjian Cheng(程二建)1, Lin Guo(郭琳)1, Binglin Pan(泮炳霖)1, Yeyu Huang(黄烨煜)1, Jiamin Ni(倪佳敏)1, Yanfeng Guo(郭艳峰)2,†, Xiaofan Yang(杨小帆)1,‡, and Shiyan Li(李世燕)1,3,4,§

Citation: Chin. Phys. B, 2022, 31 (7): 076201 DOI: 10.1088/1674-1056/ /ac7212
Journal homepage: http://cpb.iphy.ac.cn; http://iopscience.iop.org/cpb

What follows is a list of articles you may be interested in

Reaction mechanism of metal and pyrite under high-pressure and high-temperature conditions and improvement of the properties

Yao Wang(王遥), Dan Xu(徐丹), Shan Gao(高姗), Qi Chen(陈启), Dayi Zhou(周大义), Xin Fan(范鑫), Xin-Jian Li(李欣健), Lijie Chang(常立杰),Yuewen Zhang(张跃文), Hongan Ma(马红安), and Xiao-Peng Jia(贾晓鹏)
Chin. Phys. B, 2022, 31 (**6**): 066206. DOI: 10.1088/1674-1056/ac4a72

Bandgap evolution of Mg_3N_2 under pressure: Experimental and theoretical studies

Gang Wu(吴刚), Lu Wang(王璐), Kuo Bao(包括), Xianli Li(李贤丽), Sheng Wang(王升), and Chunhong Xu(徐春红)
Chin. Phys. B, 2022, 31 (**6**): 066205. DOI: 10.1088/1674-1056/ac4cbe

Structural and electrical transport properties of charge density wave material $LaAgSb_2$ under high pressure

Bowen Zhang(张博文), Chao An(安超), Xuliang Chen(陈绪亮), Ying Zhou(周颖), Yonghui Zhou(周永惠), Yifang Yuan(袁亦方), Chunhua Chen(陈春华), Lili Zhang(张丽丽), Xiaoping Yang(杨晓萍), and Zhaorong Yang(杨昭荣)
Chin. Phys. B, 2021, 30 (**7**): 076201. DOI: 10.1088/1674-1056/abf643

Utilizing of high-pressure high-temperature synthesis to enhance the thermoelectric properties of $Zn_{0.98}Al_{0.02}O$ with excellent electrical properties

Qi Chen(陈启), Xinjian Li(李欣健), Yao Wang(王遥), Lijie Chang(常立杰), Jian Wang(王健), Yuewen Zhang(张跃文), Hongan Ma(马红安), and Xiaopeng Jia(贾晓鹏)
Chin. Phys. B, 2021, 30 (**1**): 016202. DOI: 10.1088/1674-1056/abc4dd

Experimental investigation on the properties of liquid film breakup induced by shock waves

Xianzhao Song(宋先钊), Bin Li(李斌), Lifeng Xie(解立峰)
Chin. Phys. B, 2020, 29 (**8**): 086201. DOI: 10.1088/1674-1056/ab928a

---

RAPID COMMUNICATION

High-pressure study of topological semimetals XCd$_2$Sb$_2$ (X = Eu and Yb)

Chuchu Zhu(朱楚楚)[1], Hao Su(苏豪)[2], Erjian Cheng(程二建)[1], Lin Guo(郭琳)[1], Binglin Pan(泮炳霖)[1], Yeyu Huang(黄烨煜)[1], Jiamin Ni(倪佳敏)[1], Yanfeng Guo(郭艳峰)[2,†], Xiaofan Yang(杨小帆)[1,‡], and Shiyan Li(李世燕)[1,3,4,§]

[1] *State Key Laboratory of Surface Physics and Department of Physics, Fudan University, Shanghai* 200438, *China*
[2] *School of Physical Science and Technology, ShanghaiTech University, Shanghai* 201210, *China*
[3] *Collaborative Innovation Center of Advanced Microstructures, Nanjing* 210093, *China*
[4] *Shanghai Research Center for Quantum Sciences, Shanghai* 201315, *China*

(Received 17 April 2022; revised manuscript received 9 May 2022; accepted manuscript online 23 May 2022)

Topological materials have aroused great interest in recent years, especially when magnetism is involved. Pressure can effectively tune the topological states and possibly induce superconductivity. Here we report the high-pressure study of topological semimetals XCd$_2$Sb$_2$ (X = Eu and Yb), which have the same crystal structure. In antiferromagnetic (AFM) Weyl semimetal EuCd$_2$Sb$_2$, the Néel temperature (T_N) increases from 7.4 K at ambient pressure to 50.9 K at 14.9 GPa. When pressure is above 14.9 GPa, the AFM peak of resistance disappears, indicating a non-magnetic state. In paramagnetic Dirac semimetal candidate YbCd$_2$Sb$_2$, pressure-induced superconductivity appears at 1.94 GPa, then T_c reaches to a maximum of 1.67 K at 5.22 GPa and drops to zero at about 30 GPa, displaying a dome-shaped temperature–pressure phase diagram. High-pressure x-ray diffraction measurement demonstrates that a crystalline-to-amorphous phase transition occurs at about 16 GPa in YbCd$_2$Sb$_2$, revealing the robustness of pressure-induced superconductivity against structural instability. Similar structural phase transition may also occur in EuCd$_2$Sb$_2$, causing the disappearance of magnetism. Our results show that XCd$_2$Sb$_2$ (X = Eu and Yb) is a novel platform for exploring the interplay among magnetism, topology, and superconductivity.

Keywords: high pressure, topological semimetal, magnetism, superconductivity

PACS: 62.50.–p, 74.62.Fj, 75.50.Ee, 81.40.Rs **DOI:** 10.1088/1674-1056/ac7212

1. Introduction

Topological materials have been widely investigated in recent years due to their novel physical properties and the potential application in electronic devices.[1–6] By introducing magnetism into the topological materials, the initial electronic structure is modified by the broken time-reversal symmetry.[7] The combination of intrinsic magnetic order and nontrivial topology provides a platform for the investigations of exotic quantum states, such as Weyl semimetals,[8–11] anomalous Hall effect,[12,13] and axion insulators.[1,14]

In this context, the topological semimetals EuCd$_2M_2$ (M = As and Sb) have recently attracted a lot of attention due to its special A-type AFM configuration.[15–26] The Eu spins order ferromagnetically in the *ab* plane and stack antiferromagnetically along *c* axis below Néel temperature $T_N = 9.5$ K for M = As and 7.4 K for M = Sb.[15–17] First-principle theoretical calculations predicted that EuCd$_2M_2$ (M = As and Sb) is an AFM Dirac semimetal candidate with unbroken C_3 symmetry,[18] and a single pair of Weyl nodes could be generated by splitting the Dirac cone close to Fermi surface in ferromagnetic (FM) state.[19] Experimentally, in AFM phase, the EuCd$_2M_2$ was revealed to hold several nontrivial topological states including axion insulator, AFM topological crystalline insulator, and higher order topological insulator.[15,16,20] In spin-polarized FM phase induced by an external magnetic field along *c* axis, a single pair of Weyl nodes is generated near Fermi level due to the break of nonsymmetric time-reversal symmetry.[17,20] In the paramagnetic phase above T_N, quasi-static FM fluctuations lift the Kramers degeneracy, indicating a centrosymmetric Weyl semimetal state of EuCd$_2M_2$.[22] Furthermore, the magnetic order in EuCd$_2M_2$ can be suppressed by substituting europium atoms with non-magnetic atoms, for instance, ytterbium. The Yb-based compounds behave paramagnetically and the C_3 symmetry is maintained, becoming ideal Dirac semimetal candidates. Therefore, XCd$_2M_2$ (X = Eu and Yb, M = As and Sb) has provided an ideal platform for exploring the intriguing interplay between topology and magnetism.[23–25]

Applying pressure is a clean and effective method of tuning crystal structure and electronic state. Under pressure, the magnetic ordering may be suppressed and novel ground states such as superconductivity may emerge.[27–32] In this

†Corresponding author. E-mail: guoyf@shanghaitech.edu.cn
‡Corresponding author. E-mail: yangxiaofan@fudan.edu.cn
§Corresponding author. E-mail: shiyan_li@fudan.edu.cn

© 2022 Chinese Physical Society and IOP Publishing Ltd

paper, we report the high-pressure electrical transport studies on $EuCd_2Sb_2$ and $YbCd_2Sb_2$. It is found that the AFM transition temperature T_N of $EuCd_2Sb_2$ increases from 7.4 K at ambient pressure to 50.9 K at 14.9 GPa, then the magnetism disappears. No sign of superconductivity is observed down to 300 mK. In contrast, superconductivity emerges in $YbCd_2Sb_2$ at 1.94 GPa, manifesting a superconducting dome in the temperature-pressure phase diagram. High-pressure x-ray diffraction (XRD) measurements on $YbCd_2Sb_2$ show no structural phase transition at low pressure, but a crystalline-to-amorphous phase transition at about 16 GPa. Similar structural phase transition may cause the disappearance of magnetism in $EuCd_2Sb_2$.

2. Materials and methods

The $EuCd_2Sb_2$ single crystals were grown by using tin as flux.[16] High-quality single crystals of $YbCd_2Sb_2$ were grown by self-flux method using a mixture of Yb (purity 99.9%), Cd (purity 99.99%), and Sb (purity 99.999%) powders with a molar ratio of 1:20:2. The mixture was loaded into a corundum crucible which was further sealed in a quartz ampoule under vacuum. Subsequently, the ampoule was heated at 730 °C for 5000 minutes and then slowly cooled down to 430 °C at a rate of 1 °C/h. Single crystals can be obtained by removing excess flux in a centrifuge and cooling down to room temperature.

High pressure was generated by a diamond anvil cell (DAC), in which diamond anvils with a culet size of diameter 300 μm and a non-magnetic Be–Cu gasket were employed. Cubic boron nitride (c-BN) and NaCl powders were used as insulating material and pressure transmitting medium, respectively. XCd_2Sb_2 (X = Eu and Yb) single crystals were crashed into small pieces and loaded inside of a hole (120 μm in diameter) in the center of the gasket. Subsequently, four electrodes of 4-μm-thick platinum thin foils were laid on the sample. With applying pressure, the small single crystals were crashed into powder and compressed together solidly, allowing a standard ohmic contact between sample and electrodes. The solid pressure transmitting medium provides a quasi-hydrostatic condition. The pressure inside the DAC was scaled by monitoring the Ruby fluorescence at room temperature each time before and after the measurement.[33] High pressure resistance of $EuCd_2Sb_2$ and $YbCd_2Sb_2$ were measured in a physical property measurement system (PPMS, Quantum Design) and a ^{3}He cryostat with Van der Pauw method.

The XRD measurement at ambient pressure was performed by using an x-ray diffractometer (D8 Advance, Bruker). The high-pressure synchrotron XRD experiments were carried out using a symmetric DAC with a 260-μm culet diamond. A rhenium gasket was pre-compressed to 30 μm in thickness followed by drilling the central part by laser to form a 90-μm diameter hole as the sample chamber. The sample chamber was filled with a mixture of the sample, a ruby chip, and silicone oil as the pressure transmitting medium. The experimental pressures were determined by the pressure-induced fluorescence shift of ruby. Synchrotron XRD measurements were carried out at beamline BL15U1 of the Shanghai Synchrotron Radiation Facility (SSRF) using a monochromatic beam of 0.6199 Å.

3. Results and discussion

Figure 1(a) shows the crystal structure of XCd_2Sb_2 (X = Eu and Yb) at ambient pressure. XCd_2Sb_2 crystallizes in trigonal structure with a space group of $P\bar{3}m1$ (No. 164).[34,35] The ionic $[Cd_2Sb_2]$ slab is sandwiched between layers of ytterbium/europium cations along c axis. From the XRD patterns in Fig. 1(b), only (00l) Bragg peaks are detected, demonstrating that the largest natural surface of as-grown XCd_2Sb_2 single crystals is ab plane. Typical resistivity $\rho(T)$ curves of XCd_2Sb_2 single crystals at ambient pressure are plotted in Fig. 1(c). At high temperature, the resistivity of $EuCd_2Sb_2$ exhibits a metallic behavior. Below 100 K, with decreasing temperature the resistivity increases rapidly to a maximum at $T_N = 7.4$ K and then drops sharply. The low-temperature resistivity behavior of $EuCd_2Sb_2$ resembles previous report on its sister compound $EuCd_2As_2$, which attributed the sharp drop below T_N to the reduced scattering from the ordered state of the Eu moments.[23] For paramagnetic $YbCd_2Sb_2$, its resistivity exhibits a weakly metallic behavior.

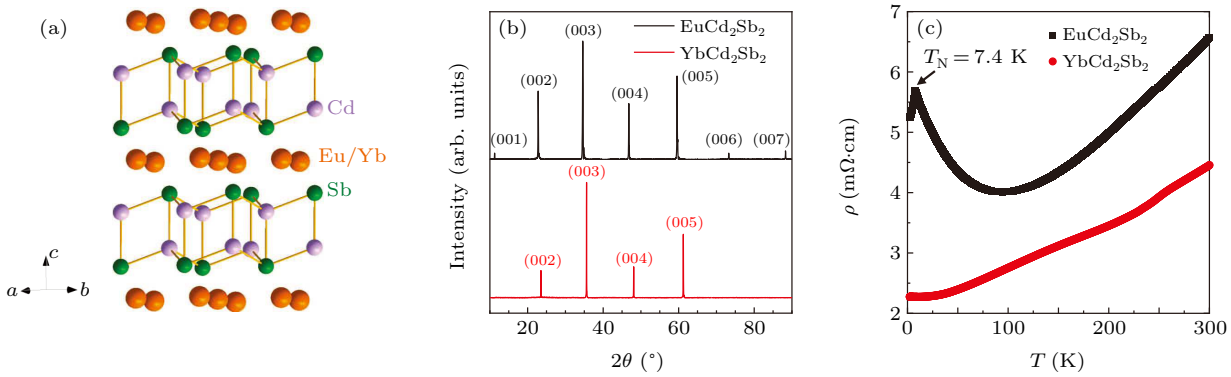


Fig. 1. (a) Schematic crystal structure of XCd_2Sb_2 (X = Eu and Yb). Green, purple, and orange balls represent Sb, Cd, and Eu/Yb atoms, respectively. (b) Room-temperature x-ray diffraction pattern of XCd_2Sb_2 (X = Eu and Yb) single crystals, showing that the largest natural surface is ab plane. (c) Typical resistivity curves of XCd_2Sb_2 (X = Eu and Yb) single crystals at ambient pressure. The peak at 7.4 K denotes the antiferromagnetic transition of $EuCd_2Sb_2$.

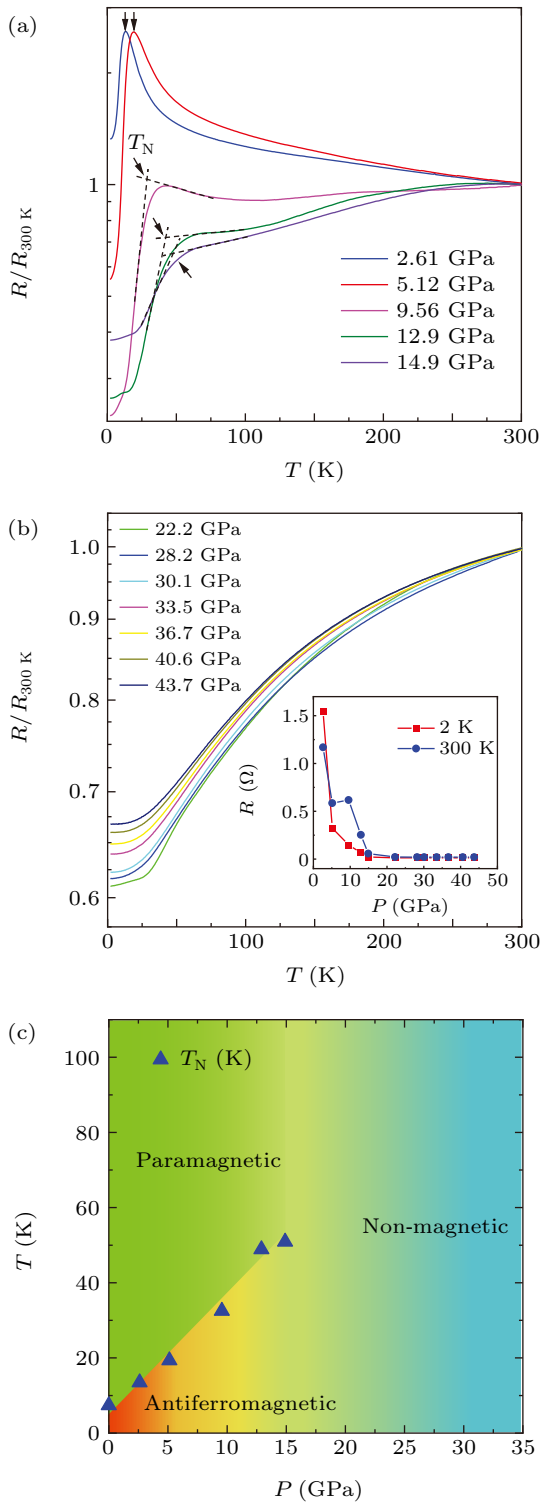


Fig. 2. Temperature dependence of the normalized resistance under different pressures for $EuCd_2Sb_2$ (a) below 14.9 GPa and (b) above 14.9 GPa in a temperature range of 2 K–300 K, respectively. The arrows denote the Néel temperature T_N. The inset of (b) depicts the pressure dependence of R at $T = 2$ K (red squares) and 300 K (blue circles). (c) The temperature–pressure phase diagram of $EuCd_2Sb_2$. The values of T_N are obtained from panel (a).

Figures 2(a) and 2(b) present the temperature-dependence normalized resistance $R/R_{300\,K}$ of $EuCd_2Sb_2$ up to 43.7 GPa. The data are obtained from two samples with two experimental runs, which have consistent results. The application of 2.61 GPa and 5.12 GPa shift T_N (the peak position) towards higher values. For 9.56 GPa and above, the AFM peak becomes broader and lower, therefore we redefine the value of T_N as the point of intersection of two lines extrapolated from the $R(T)$ curve below and above the temperatures of the broad peak. The value of T_N increases substantially to a maximum of 50.9 K at 14.9 GPa, about 6.8 times of that at ambient pressure. When the pressure is above 14.9 GPa, the AFM peak completely vanishes, indicating the absence of magnetic phase transition. The absolute resistances $R_{2\,K}$ and $R_{300\,K}$ also decrease to very small values, as shown in the inset of Fig. 2(b). From these results, we construct the temperature-pressure phase diagram of $EuCd_2Sb_2$ in Fig. 2(c). There are two main features in the phase diagram: (i) T_N increases monotonously with the applied pressure up to 14.9 GPa, then drops to zero. A similar phase diagram has recently been reported in $EuIn_2As_2$, in which the increase of T_N is mainly attributed to the enhancement of intralayer ferromagnetic exchange coupling by pressure.[36] (ii) A non-magnetic state appears after the collapse of AFM phase above 14.9 GPa. Similarly, for $EuIn_2As_2$, with increasing pressure up to 17 GPa, a crystalline-to-amorphous phase transition occurs, which impedes further enhancement of T_N.[36] This will be discussed later. In order to further check whether there is pressure-induced superconductivity in $EuCd_2Sb_2$, we also measure another sample down to 300 mK and no sign of superconductivity is observed (data not shown here).

The resistance $R(T)$ from 0.3 K to 300 K for $YbCd_2Sb_2$ sample A under pressures up to 29.2 GPa is plotted in Fig. 3(a). At low temperature, a resistance drop is clearly observed under 1.94 GPa, and becomes more pronounced with increasing pressure, as shown in Fig. 3(b). The value of T_c (defined at the 10% drop of normal-state resistance, $T_c^{10\%}$), first increases to a maximum of 1.67 K at 5.22 GPa then decreases, eventually drops to below 0.3 K at 29.2 GPa. Noting that no zero resistance is observed for $YbCd_2Sb_2$ sample A in the whole pressure range. To confirm that the R drop is due to superconducting transition, we measure the resistance of sample A at different magnetic fields under 10.0 GPa. The R drop is gradually suppressed upon increasing magnetic field and completely disappears at 0.6 T. The upper critical field $\mu_0 H_{c2}(T)$ as a function of temperature is extracted and plotted in the inset of Fig. 3(c). It can be well fitted by the empirical Ginzburg–Landau (GL) formula[37]

$$\mu_0 H_{c2}(T) = \mu_0 H_{c2}(0)(1-(T/T_c)^2)(1+(T/T_c)^2). \quad (1)$$

The zero-temperature upper critical field $\mu_0 H_{c2}(0)$ is determined to be 0.41 T, which is much lower than the Pauli paramagnetic limit field $H_p(0) = 1.84 T_c \approx 1.86$ T,[38,39] indicating the absence of Pauli pair breaking.

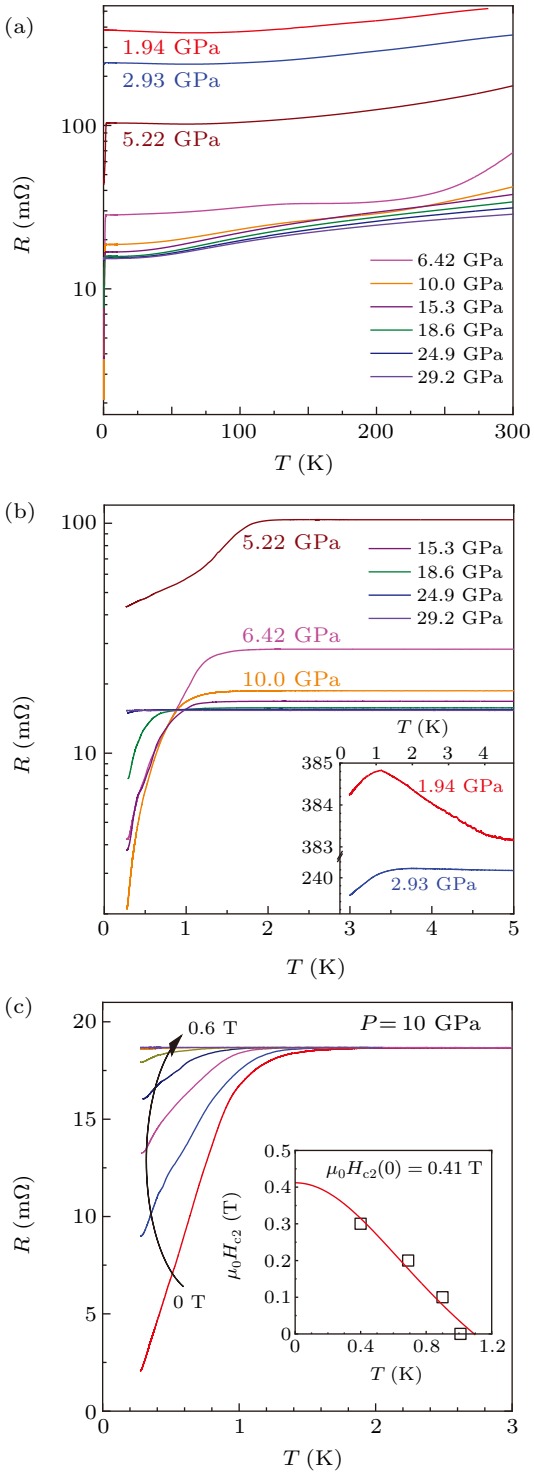


Fig. 3. High-pressure resistance curves of $YbCd_2Sb_2$ sample A. (a) Temperature dependence of resistance under different pressures up to 300 K. (b) Low-temperature resistance shows the superconducting transition. The inset in panel (b) demonstrates that pressure-induced superconductivity emerges at 1.94 GPa. (c) Temperature dependence of resistance at different magnetic fields under 10.0 GPa. The superconducting transition temperature T_c is defined at the 10% drop of normal-state resistance ($T_c^{10\%}$). The inset in panel (c) depicts the upper critical field $\mu_0 H_{c2}$ as a function of T_c, which can be well fitted by Ginzburg–Landau formula.

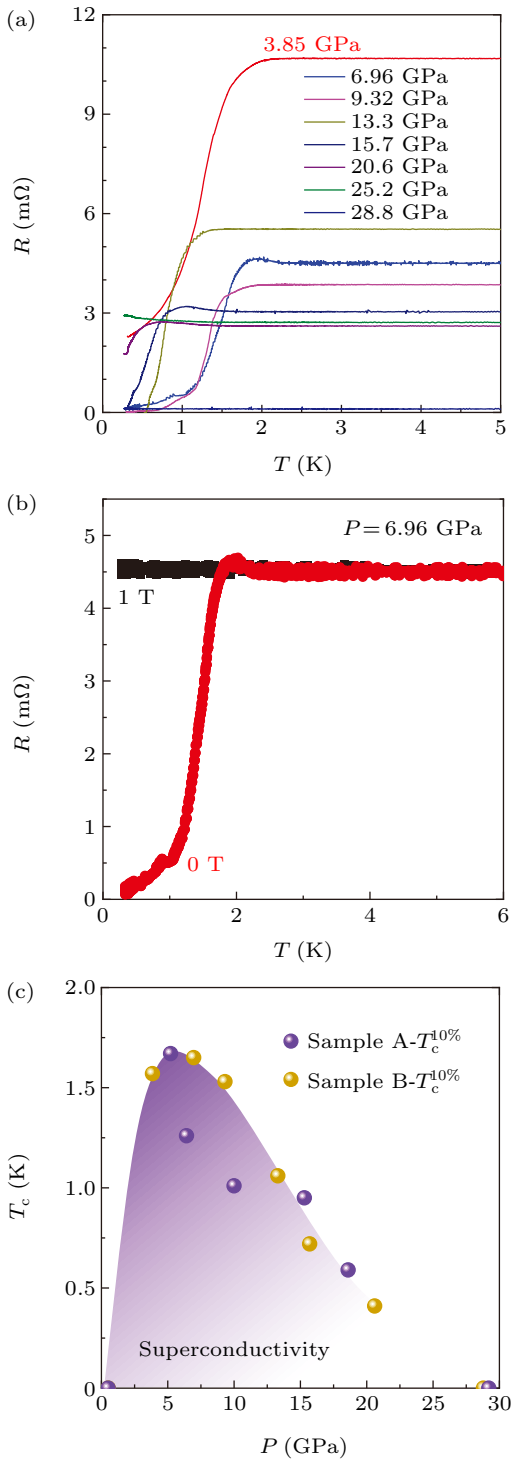


Fig. 4. (a) Low-temperature resistance under different pressures for $YbCd_2Sb_2$ sample B. (b) Temperature dependence of resistance under 0 T and 1 T at 6.96 GPa. (c) Temperature–pressure phase diagram of $YbCd_2Sb_2$, showing a dome-shaped pressure-induced superconductivity.

In order to reproduce the pressure-induced superconductivity in $YbCd_2Sb_2$, a new sample B obtained from a different batch was measured under pressures from 3.85 GPa to 28.8 GPa, as shown in Fig. 4(a). For sample B, zero resistance is observed and the highest T_c is 1.65 K under 6.96 GPa, consistent with sample A. When an external field 1 T is applied, the R drop of sample B under 6.96 GPa is completely suppressed, as shown in Fig. 4(b). These results confirm the pressure-induced superconductivity in $YbCd_2Sb_2$. Combining the results of sample A with sample B, the temperature–pressure phase diagram of $YbCd_2Sb_2$ is mapped out in Fig. 4(c), which shows a clear superconducting

dome. Note that the data points of 24.9 GPa for sample A and 25.2 GPa for sample B are not shown, since the T_cs are below our lowest temperature 0.3 K. For the data points of 29.2 GPa for sample A and 28.8 GPa for sample B, we estimate that the T_cs are very close to zero. These do not affect the overall shape of the superconducting dome in Fig. 4(c).

To check whether the pressure-induced superconductivity arises from a structural phase transition, we performed high-pressure synchrotron XRD measurements on $YbCd_2Sb_2$ sample, shown in Fig. 5(a) for different pressures. The ambient–pressure phase persists up to 12.3 GPa, since no new diffraction peaks appear. Therefore, the superconductivity in $YbCd_2Sb_2$ is not related to a pressure-induced structural phase transition. The pressure dependence of lattice parameters a, b, and unit-cell volume V/Z are plotted in Figs. 5(b) and 5(c), obtained by fitting the XRD data with GSAS software. There is no anomaly in a, b, and V/Z except that the volume is compressed by 15.3%. Below 12.3 GPa, the evolution of V/Z can be well fitted by Birch–Murnaghan equation[40]

$$P = \frac{3}{2}B_0\left[\left(\frac{V_0}{V}\right)^{7/3} - \left(\frac{V_0}{V}\right)^{5/3}\right] \times\left\{1+\frac{3}{4}\left(B_0'-4\right)\left[\left(\frac{V_0}{V}\right)^{2/3}-1\right]\right\}, \quad (2)$$

where B_0, B_0', and V_0 are the bulk modulus, first-order derivative of the bulk modulus, and the derived zero-pressure volume, respectively. The fitting gives $V_0 = 145.2$ Å^3, $B_0 = 34.6$ GPa, and $B_0' = 9.1$.

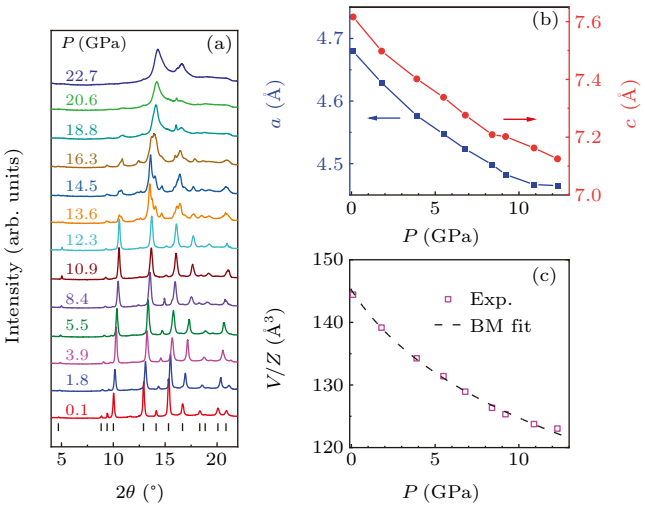


Fig. 5. (a) High-pressure x-ray diffraction ($\lambda = 0.6199$ Å) patterns of $YbCd_2Sb_2$ under pressures ranging from 0.1 GPa to 22.7 GPa. (b) and (c) Pressure dependence of the lattice parameters a, c, and V/Z for $YbCd_2Sb_2$, respectively. The black dashed line is the fitting of third-order Birch–Murnaghan equation, which derives zero-pressure volume $V_0 = 145.2$ Å^3, bulk modulus $B_0 = 34.6$ GPa, and the first-order derivative of the bulk modulus $B_0' = 9.1$.

Above 12.3 GPa, the pristine trigonal phase still exists, but the peak intensity decreases and some small diffraction peaks appear around major splitting peaks, which is resembling of $EuCd_2As_2$,[41] suggesting the instability of crystal structure and the emergence of new phase. However, it is hard to determine the space group of the high-pressure phase due to the complex diffraction spectra. When the pressure is higher than 16.3 GPa, the original diffraction peaks gradually vanish and only two humps are detected at 22.7 GPa. This is reminiscent of the crystalline-to-amorphous phase transition in $EuIn_2As_2$ at $\sim$ 17 GPa.[36] For $YbCd_2Sb_2$, the superconductivity persists into the amorphous phase. Considering the structure similarity of $EuCd_2Sb_2$, $YbCd_2Sb_2$, and $EuIn_2As_2$, such crystalline-to-amorphous phase transition should also occur in $EuCd_2Sb_2$. Since the amorphous phase has no lattice period thus absence of magnetic order, this may explain the sudden disappearance of AFM order around 14.9 GPa in $EuCd_2Sb_2$. On the other hand, considering the energy difference between divalent and trivalent Eu ionic state is not extremely large and the ion radius of Eu^{3+} is smaller than Eu^{2+}, Eu^{2+} state could thus be easily destabilized and pushed towards Eu^{3+} state with external energy like pressurization in some Eu-based compounds,[42] leading to the collapse of antiferromagnetism. Whereas we did not detected the thermal hysteresis on cooling and warming resistance curves (as a hallmark of valence transition),[43–45] more high-pressure x-ray photoemission spectroscopy (XPS), x-ray absorption near-edge spectroscopy (XANES), and XRD measurements that could directly monitor valence and structure transition are further needed.

The superconducting dome found in $YbCd_2Sb_2$ is quite interesting. Usually, such a superconducting dome is associated with the suppression of magnetic order[46] or charge-density wave.[47] However, no magnetic order and charge-density wave have been observed in $YbCd_2Sb_2$. In this sense, its superconducting dome may be due to a Lifshitz transition (related to electrical topological transition and Fermi surface reconstruction), as observed in WTe_2.[28] More Hall coefficient measurement on single crystal and electronic band structure calculation under pressure are needed to further clarify this issue.

4. Conclusion

We have systematically measured the resistance of topological semimetals XCd_2Sb_2 (X = Eu and Yb) under high pressures. For $EuCd_2Sb_2$, it is found that pressure strongly enhances the AFM transition up to $\sim$ 15 GPa, then the magnetic order suddenly disappears. The increase of T_N is attributed to pressure-enhanced intralayer FM exchange coupling and a crystalline-to-amorphous phase transition may cause the disappearance of magnetic order. For paramagnetic $YbCd_2Sb_2$, a clear superconducting dome is observed in the temperature–pressure phase diagram, which may relate to some kind of

Lifshitz transition. Our results demonstrate that XCd$_2$Sb$_2$ (X = Eu and Yb) is a novel platform for exploring the interplay among magnetism, topology and superconductivity.

Acknowledgments

Project supported by the National Natural Science Foundation of China (Grant No. 12174064) and the Shanghai Municipal Science and Technology Major Project (Grant No. 2019SHZDZX01). Yanfeng Guo acknowledges the research fund from the State Key Laboratory of Surface Physics and Department of Physics, Fudan University (Grant No. KF2020_09).

References

[1] Zhang D, Shi M, Zhu T, Xing D, Zhang H and Wang J 2019 *Phys. Rev. Lett.* **122** 206401
[2] Li H, He H, Lu H Z, Zhang H, Liu H, Ma R, Fan Z, Shen S Q and Wang J 2016 *Nat. Commun.* **7** 10301
[3] Wu L, Patankar S, Morimoto T, Nair N L, Thewalt E, Little A, Analytis J G, Moore J E and Orenstein J 2017 *Nat. Phys.* **13** 350
[4] He Q L, Pan L, Stern A L, Burks E C, Che X, Yin G, Wang J, Lian B, Zhou Q, Choi E S, Murata K, Kou X, Chen Z, Nie T, Shao Q, Fan Y, Zhang S C, Liu K, Xia J and Wang K L 2017 *Science* **357** 294
[5] Xu S Y, Liu C, Kushwaha S K, Sankar R, Krizan J W, Belopolski I, Neupane M, Bian G, Alidoust N, Chang T R, Jeng H T, Huang C Y, Tsai W F, Lin H, Shibayev P P, Chou F C, Cava R J and Hasan M Z 2015 *Science* **347** 294
[6] Mogi M, Kawamura M, Yoshimi R, Tsukazaki A, Kozuka Y, Shirakawa N, Takahashi K S, Kawasaki M and Tokura Y 2017 *Nat. Mater.* **16** 516
[7] Chen Y L, Chu J H, Analytis J G, Liu Z K, Igarashi K, Kuo H H, Qi X L, Mo S K, Moore R G, Lu D H, Hashimoto M, Sasagawa T, Zhang S C, Fisher I R, Hussain Z and Shen Z X 2010 *Science* **329** 659
[8] Huang L, McCormick T M, Ochi M, Zhao Z, Suzuki M T, Arita R, Wu Y, Mou D, Cao H, Yan J, Trivedi N and Kaminski A 2016 *Nat. Mater.* **15** 1155
[9] Xu S Y, Belopolski I, Alidoust N, Neupane M, Bian G, Zhang C, Sankar R, Chang G, Yuan Z, Lee C C, Huang S M, Zheng H, Ma J, Sanchez D S, Wang B, Bansil A, Chou F, Shibayev P P, Lin H, Jia S and Hasan M Z 2015 *Science* **349** 613
[10] Borisenko S, Evtushinsky D, Gibson Q, Yaresko A, Koepernik K, Kim T, Ali M, van den Brink J, Hoesch M, Fedorov A, Haubold E, Kushnirenko Y, Soldatov I, Schafer R and Cava R J 2019 *Nat. Commun.* **10** 3424
[11] Bulmash D, Liu C X and Qi X L 2014 *Phys. Rev. B* **89** 081106
[12] Xu G, Weng H, Wang Z, Dai X and Fang Z 2011 *Phys. Rev. Lett.* **107** 186806
[13] Hosur P and Qi X 2013 *Comp. Rend. Phys.* **14** 857
[14] Xu Y, Song Z, Wang Z, Weng H and Dai X 2019 *Phys. Rev. Lett.* **122** 256402
[15] Rahn M C, Soh J R, Francoual S, Veiga L S I, Strempfer J, Mardegan J, Yan D Y, Guo Y F, Shi Y G and Boothroyd A T 2018 *Phys. Rev. B* **97** 214422
[16] Soh J R, Donnerer C, Hughes K M, Schierle E, Weschke E, Prabhakaran D and Boothroyd A T 2018 *Phys. Rev. B* **98** 064419
[17] Soh J R, de Juan F, Vergniory M G, Schröter N B M, Rahn M C, Yan D Y, Jiang J, Bristow M, Reiss P, Blandy J N, Guo Y F, Shi Y G, Kim T K, McCollam A, Simon S H, Chen Y, Coldea A I and Boothroyd A T 2019 *Phys. Rev. B* **100** 201102
[18] Hua G, Nie S, Song Z, Yu R, Xu G and Yao K 2018 *Phys. Rev. B* **98** 201116
[19] Wang L L, Jo N H, Kuthanazhi B, Wu Y, McQueeney R J, Kaminski A and Canfield P C 2019 *Phys. Rev. B* **99** 245147
[20] Ma J, Wang H, Nie S, Yi C, Xu Y, Li H, Jandke J, Wulfhekel W, Huang Y, West D, Richard P, Chikina A, Strocov V N, Mesot J, Weng H, Zhang S, Shi Y, Qian T, Shi M and Ding H 2020 *Adv. Mater.* **32** 1907565
[21] Su H, Gong B, Shi W, Yang H, Wang H, Xia W, Yu Z, Guo P J, Wang J, Ding L, Xu L, Li X, Wang X, Zou Z, Yu N, Zhu Z, Chen Y, Liu Z, Liu K, Li G and Guo Y 2020 *APL Mater.* **8** 011109
[22] Ma J Z, Nie S M, Yi C J, Jandke J, Shang T, Yao M Y, Naamneh M, Yan L Q, Sun Y, Chikina A, Strocov V N, Medarde M, Song M, Xiong Y M, Xu G, Wulfhekel W, Mesot J, Reticcioli M, Franchini C, Mudry C, Müller M, Shi Y G, Qian T, Ding H and Shi M 2019 *Sci. Adv.* **5** eaaw4718
[23] Wang H P, Wu D S, Shi Y G and Wang N L 2016 *Phys. Rev. B* **94** 045112
[24] Xu Y, Das L, Ma J Z, Yi C J, Nie S M, Shi Y G, Tiwari A, Tsirkin S S, Neupert T, Medarde M, Shi M, Chang J and Shang T 2021 *Phys. Rev. Lett.* **126** 076602
[25] Niu C, Mao N, Hu X, Huang B and Dai Y 2019 *Phys. Rev. B* **99** 235119
[26] Wang Y, Li C, Li Y, Zhou X B, Wu W, Yu R Z, Zhao J F, Yin C H, Shi Y G, Jin C Q, Luo J L, Zhao L, Xiang T, Liu G D and Zhou X J 2021 *Chin. Phys. Lett.* **38** 077201
[27] Pan X C, Chen X L, Liu H M, Feng Y Q, Wei Z X, Zhou Y H, Chi Z H, Pi L, Yen F, Song F Q, Wan X G, Yang Z R, Wang B G, Wang G H and Zhang Y H 2015 *Nat. Commun.* **6** 7805
[28] Kang D F, Zhou Y Z, Yi W, Yang C L, Guo J, Shi Y G, Zhang S, Wang Z, Zhang C, Jiang S, Li A G, Yang K, Wu Q, Zhang G M, Sun L L and Zhao Z X 2015 *Nat. Commun.* **6** 7804
[29] He L, Jia Y, Zhang S, Hong X, Jin C and Li S 2016 *npj Quantum Mater.* **1** 16014
[30] Cheng E, Xia W, Shi X, Yu Z, Wang L, Yan L, Peets D C, Zhu C, and Su H, Zhang Y, Dai D, Wang X, Zou Z, Yu N, Kou X, Yang W, Zhao W, Guo Y and Li S 2020 *npj Quantum Mater.* **5** 38
[31] Sun L L, Chen X J, Guo J, Gao P W, Huang Q Z, Wang H D, Fang M H, Chen X L, Chen G F, Wu Q, Zhang C, Gu D C, Dong X L, Wang L, Yang K, Li A G, Dai X, Mao H k and Zhao Z X 2012 *Nature* **483** 67
[32] Li Y, An C, Hua C, Chen X, Zhou Y, Zhou Y, Zhang R, Park C, Wang Z, Lu Y, Zheng Y, Yang Z and Xu Z A 2018 *npj Quantum Mater.* **3** 58
[33] Mao H K, Bell P M, Shaner J W and Steinberg D J 1978 *J. Appl. Phys.* **49** 3276
[34] Artmann A, Mewis A, Roepke M and Michels G 1996 *Z. Anorg. Allg. Chem.* **622** 679
[35] Zhang H, Fang L, Tang M B, Man Z Y, Chen H H, Yang X X, Baitinger M, Grin Y and Zhao J T 2010 *J. Chem. Phys.* **133** 194701
[36] Yu F H, Mu H M, Zhuo W Z, Wang Z Y, Wang Z F, Ying J J and Chen X H 2020 *Phys. Rev. B* **102** 180404
[37] Landau L and Ginzburg V 1950 *Zh. Eksp. Teor. Fiz.* **20** 1064
[38] Clogston A M 1962 *Phys. Rev. Lett.* **9** 266
[39] Chandrasekhar B S 1962 *Appl. Phys. Lett.* **1** 7
[40] Birch F 1974 *Phys. Rev.* **71** 809
[41] Yu Z, Chen X, Xia W, Wang N, Lv X, Liu X, Su H, Li Z, Wu D, Wu W, Liu Z, Zhao J, Li M, Li S, Li X, Dong Z, Zhou C, Zhang L, Wang X, Yu N, Zou Z, Luo J, Cheng J, Wang L, Zhong Z and Guo Y 2022 arXiv: 2202.06016
[42] ōnuki Y, Nakamura A, Honda F, Aoki D, Tekeuchi T, Nakashima M, Amako Y, Harima H, Matsubayashi K, Uwatoko Y, Kayama S, Kagayama T, Shimizu K, Esakki Muthu S, Braithwaite D, Salce B, Shiba H, Yara T, Ashitomi Y, Akamine H, Tomori K, Hedo M and Nakama T 2017 *Philos. Mag.* **97** 3399
[43] Seiro S and Geibel C 2011 *J. Phys.: Condens. Matter* **23** 375601
[44] Honda F, Okauchi K, Nakamura A, Li D, Aoki D, Akamine H, Ashitomi Y, Hedo M, Nakama T and ōnuki Y 2016 *J. Phys. Soc. Jpn.* **85** 063701
[45] Wada H, Hundley M F, Movshovich R and Thompson J D 1999 *Phys. Rev. B* **59** 1141
[46] Norman M R 2011 *Science* **332** 196
[47] Zhu C C, Yang X F, Xia W, Yin Q W, Wang L S, Zhao C C, Dai D Z, Tu C P, Song B Q, Tao Z C, Tu Z J, Gong C S, Lei H C, Guo Y F and Li S Y 2022 *Phys. Rev. B* **105** 094507